Department of Physics and Astronomy
Heidelberg University

Bachelor Thesis in Physics
submitted by

Jannis Himmelsbach

born in Freiburg i. Br. (Germany)

2022

Completion and commissioning of an LVAP ion source

This Bachelor Thesis has been carried out by
Jannis Himmelsbach
at the
Max-Planck-Institut für Kernphysik in Heidelberg
under the supervision of
Prof. Dr. Andreas Wolf

Completion and commissioning of an LVAP ion source

Cooling processes and especially the processes of delayed electron emission and delayed atom emission of clusters in the gas phase have been subject to research for the past decades. For the anionic Al_4^- clusters, a lot was learned about their cooling processes in room-temperature experiments. Much less is known about their cooling behaviour at ambient temperatures far below room temperature. Suitable experimental conditions for further studies can be provided by the Cryogenic Storage Ring (CSR). It is a cryogenic electrostatic ion storage ring, which is capable of storing ion beams in an ultracold environment with very low vacuum pressure. In order to produce cold cluster ions for the CSR, a new versatile Laser VAPorization (LVAP) ion source was designed. With this ion source, the cluster ions can be produced in already low rovibrational states. In this thesis, the LVAP ion source was taken into operation as a first step towards production of cold Al_4^- clusters and monitoring their cooling processes. The ion source and its auxiliary equipment were assembled and set up at the Ion Source Test Bench (ISTB). All necessary tests and alignment steps were successfully performed. A roadmap of measurement steps required for commissioning the LVAP ion source was developed. The first step of the commissioning process was concluded and the production of rather stable and short (about 25 µs) ion pulses was achieved.

Fertigstellen und Kommissionieren einer LVAP-Ionenquelle

Seit Jahrzehnten sind Abkühlungsprozesse und insbesondere die Prozesse der verzögerten Elektronenemission und verzögerten Atomemission von Clustern in der Gasphase Forschungsgegenstand. In Experimenten bei Raumtemperatur wurde viel über die Abkühlungsprozesse von anionischen Al_4^--Clustern in Erfahrung gebracht. Über das Abkühlverhalten bei Umgebungstemperaturen deutlich unter Raumtemperatur ist weit weniger bekannt. Geeignete experimentelle Bedingungen für weitergehende Studien sind am kryogenen Speicherring (CSR) gegeben. Dieser rein elektrostatische Ionenspeicherring ist in der Lage, Ionenstrahlen in einer ultrakalten Umgebung mit sehr niedrigem Restgasdruck zu speichern. Zur Erzeugung kalter Clusterionen für den CSR wurde eine neue Laserverdampfungsionenquelle (LVAP-Ionenquelle) entwickelt, die die Produktion von Clusterionen bereits in niedrigen Schwingungszuständen möglich macht. Im Rahmen dieser Arbeit wurde die LVAP-Ionenquelle als erster Schritt zur Herstellung von kalten Al_4^--Clustern und zur Überwachung ihrer Abkühlungsprozesse in Betrieb genommen. Die Ionenquelle und ihr Zubehör wurden am Ionenquellenteststand (ISTB) aufgebaut und eingerichtet. Alle erforderlichen Tests und Justierungsschritte wurden erfolgreich durchgeführt. Zur Inbetriebnahme der LVAP-Ionenquelle wurde eine Roadmap für die notwendigen Messschritte entwickelt. Der erste Schritt der Inbetriebnahme wurde abgeschlossen und es wurden relativ konstante und kurze (etwa 25 µs) Ionenpulse erzeugt.

Contents

1 Introduction **1**
- 1.1 The Cryogenic Storage Ring (CSR) . . . 1
- 1.2 Motivation for an LVAP ion source at the CSR . . . 2

2 Functionality of an LVAP ion source **4**

3 The LVAP ion source and its infrastructure **6**
- 3.1 Design criteria for the source setup . . . 6
- 3.2 The modified LVAP ion source . . . 6
  - 3.2.1 Ablation target . . . 9
  - 3.2.2 Ablation Laser . . . 10
  - 3.2.3 Gas system . . . 11
  - 3.2.4 Electric potentials . . . 11
  - 3.2.5 Extraction . . . 11
  - 3.2.6 Trigger timings . . . 12
- 3.3 The ion source rack . . . 12
- 3.4 The Ion Source Test Bench . . . 13
  - 3.4.1 Ion optical elements . . . 15
  - 3.4.2 Ion detection . . . 15

4 Commissioning an LVAP ion source **17**
- 4.1 Necessary tests and alignment steps prior to commissioning . . . 17
- 4.2 Roadmap for commissioning the LVAP ion source . . . 19

5 Data analysis **25**
- 5.1 Timetrace interpretation . . . 27
  - 5.1.1 The electron signal . . . 27
  - 5.1.2 The ionic signal . . . 27
- 5.2 Piezo delay for optimal signal yield . . . 29

6 Conclusion and outlook **32**

List of acronyms

CSR	Cryogenic Storage Ring
ESI	ElectroSpray Ionization
FWHM	Full Width at Half Maximum
ISTB	Ion Source Test Bench
LVAP	Laser VAPorization
MPIK	Max-Planck-Institut für Kernphysik
MISS	Metal Ion Sputter Source
PD	Piezo Delay

1 Introduction

Over the past decades, neutral and charged clusters have become of special interest in a broad range of both physics and chemistry research. They combine molecular properties and properties similar to solid bodies [1]. Their high ratio of cluster surface compared to the number of constituents makes clusters especially interesting when studying surface structures of solid bulk matter. As nanoparticles, they are of interest to the nanotechnology industry [1]. For the chemical industry, clusters serve as models for heterogeneous catalysts [2]. Understanding the intrinsic properties of these complex particles is therefore crucial for future advancements in many fields.

Among other cooling processes, delayed electron emission and delayed atom emission of clusters in the gas phase have been subject to research for the past decades [3, 4]. With new and more sophisticated methods constantly being developed, these topics continue being an object of extensive research [5]. For instance, the smallest anionic aluminium cluster showing delayed electron emission, namely Al_4^-, is very well suited for these measurements [6]. Its negative charge combined with its low mass allow storage over long time periods in both electrostatic and electromagnetic storage devices [6]. During the past couple of years, for hot Al_4^- cluster anions, a lot was learned about their cooling processes in room-temperature experiments [4, 7]. Much less is known about their cooling behaviour in lower excitation states, which are accessible in experiments carried out at very low temperatures.

1.1 The Cryogenic Storage Ring (CSR)

At Max-Planck-Institut für Kernphysik (MPIK) in Heidelberg, clusters were studied before [8, 9] and will continue to be studied in the near future. With the Cryogenic Storage Ring (CSR) facility being completed, a new possibility for storing ionic clusters in an ultracold environment with very low vacuum pressure has emerged.

The purely electrostatic ion storage ring CSR operates at cryogenic temperatures below 10 K, allowing for storage of charged particles without an upper mass limit of the stored particles [10]. The CSR is suitable for storing atomic, molecular or cluster ion beams with kinetic energies between 20 keV and 300 keV per elementary charge. Operating at a room-temperature equivalent pressure on the order of 10^{-14} mbar, this setup allows the storage of ion beams up to hours, which enables the study of slow physical processes [11]. The ring with its nearly quadratic layout and a closed-orbit circumference of approximately 35 m houses several experimental setups in the field free straight sections (figure 1.1). These include an electron cooler as well as sections for merging the ion beam with either a beam of neutral particles or laser beams. A reaction microscope, which allows to cross the stored ion beam with a jet of neutral

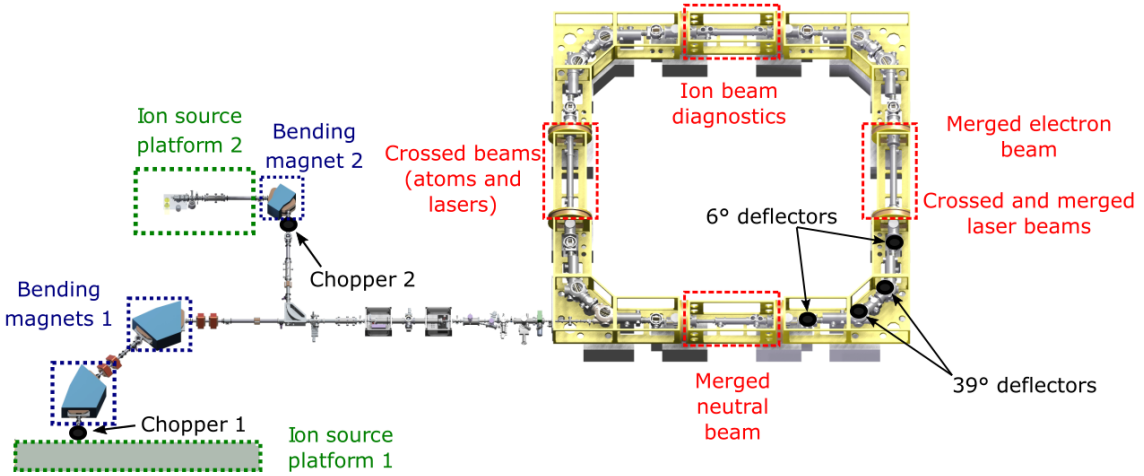

Figure 1.1: Schematic overview of the CSR and its ion source platforms. Platform 1 can be ramped up to a voltage of ±300 kV, platform 2 up to a voltage of ±60 kV. Adapted from [12].

gas atoms, will be implemented in the near future.

On the high voltage ion source platforms of the CSR, several different ion sources are used to provide a broad range of positive and negative ion beams. After acceleration of the ions to the desired final velocity, magnets are used for selecting the ion species of interest by their mass-to-charge ratio. The ion beam is then transported to and injected into the CSR. In order to control the fraction of the ring filled with ions, the ion beam can additionally be chopped using choppers and a gating electrode. A broad variety of ion sources is used or foreseen to be operated on the platforms, among them are a Heinicke type Penning source [13] for production of positive ions, an ElectroSpray Ionization (ESI) source for production of biomolecules, and a Metal Ion Sputter Source (MISS) [14] for production of negative ions or anionic clusters.

1.2 Motivation for an LVAP ion source at the CSR

While the MISS can be used for production of anionic clusters, another source to fulfil the need for cationic clusters is required. An Laser VAPorization (LVAP) ion source can produce clusters with both positive and negative charge, simply by switching the polarity of the voltages applied to the ion source chamber and extraction elements. Equally important, the internal temperature of the ions produced in a MISS is far above room temperature, whereas an LVAP source is able to produce clusters in low rovibrational states, as shown before [9]. Recently, the MISS was used for measurements of the cooling processes of Al_4^- clusters stored in the CSR. The experimental

findings are currently being analysed. Since the anionic clusters are very hot when injected into the storage ring, another measurement is planned, with Al_4^- clusters injected into the CSR already in low rovibrational states. With this measurement, it would be possible to study the course of the cooling processes reaching even further down in temperature than achieved after the longest storage times with the present MISS.

For this and other similar measurements, a new LVAP ion source was developed over the past years in a collaboration between F. Nüßlein from MPIK and the group of G. Niedner-Schatteburg at the Department of Chemistry at Technische Universität Kaiserslautern. In the course of the present work, this LVAP ion source and its auxiliary equipment is set up at the Ion Source Test Bench (ISTB), which is an experimental setup specialized on the commissioning of ion sources. The ion source is commissioned and prepared for delivering high enough output of Al_4^- for its usage at CSR.

In chapter 2 of this thesis, the functionality of an LVAP source is explained. Afterwards, the design criteria for the LVAP ion source are discussed and the experimental setup used for the commissioning process is presented (chapter 3). In chapter 4, the necessary steps for taking the setup into operation are described and a roadmap for the commissioning of the ion source is developed. The data obtained during the first measurements with the LVAP source is analysed in chapter 5. At last, a conclusion and an outlook are given in chapter 6.

2 Functionality of an LVAP ion source

LVAP sources were simultaneously developed by Smalley et al. [15] and by Bondybey and English [16]. They are extremely versatile cluster sources since they can be operated with almost every ablatable solid and can produce neutral clusters as well as anionic and cationic clusters [17]. Today, LVAP sources exist with a variety of design and geometry features specialized on the production of clusters that mainly differ in number, size, composition, charge state and temperature [17].

Focusing a laser beam with high enough power density onto the surface of solid materials leads to vaporization at the irradiated area. A hot plasma is ignited, consisting of electrons, ions and atoms of the ablated solid. For ablation to occur, the power density of the laser must be higher than the ablation threshold. The latter is strongly dependent on target material and laser wavelength [18]. Particularly high power densities can be reached with nanosecond pulsed lasers with pulse energies on the order of mJ, which are therefore preferably used for target ablation. Rotation of the target is necessary to prevent burning a hole into the ablation target by repeatedly hitting the same spot, since metal vapour would not be ejected efficiently from the hole [17].

A high pressure gas pulse then flushes the hot plasma towards the growth channel. As the name indicates, this is the place where cluster growth happens. A first expansion step takes place in the growth channel, but the gas is still constrained by the channel to promote particle collisions. When two of the target particles collide, they could form a dimer, but since the binding energy is not removed, the dimer is not stable. Therefore, a three-body-interaction with a particle of the expansion gas is necessary for the initial dimer formation [17]. In consecutive steps, collisions with other target particles lead to condensation of clusters. Repeated collisions with expansion gas particles are necessary for cooling the cluster and enabling further condensation. The gas itself cools by expansion inside the growth channel and when exiting the growth channel by supersonic expansion into the vacuum.

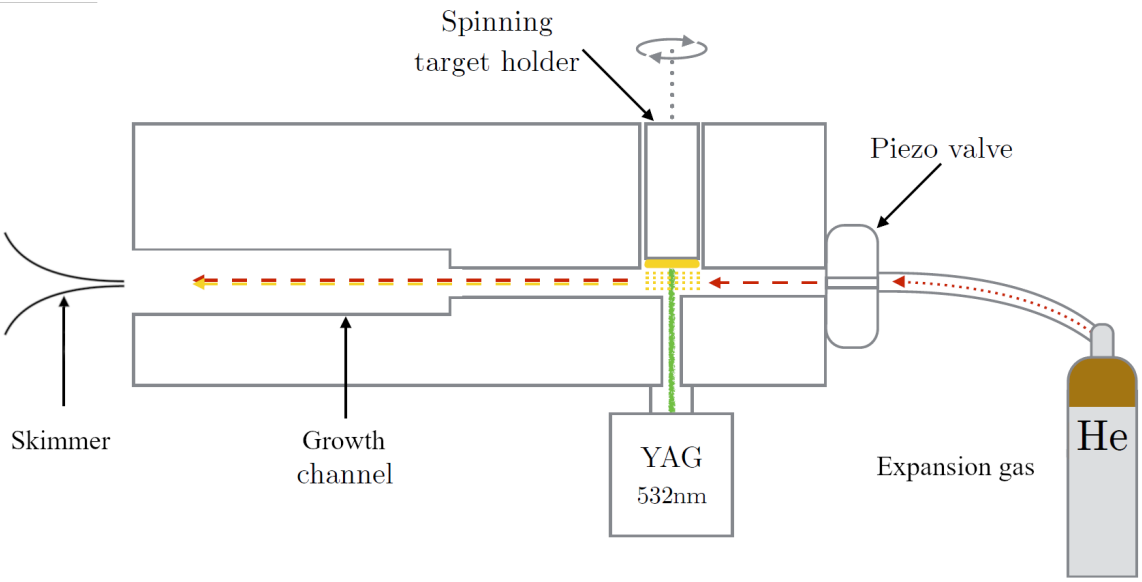

Figure 2.1: Schematic overview of an LVAP source. The red dotted arrow represents the expansion gas, the red dashed arrow shows the gas pulse. The yellow bar stands for the ablation target and the yellow dots for the ablated material. The yellow dashed arrow represents the plasma flushed with the expansion gas pulse. The green line shows the ablation laser beam. Adapted from [19].

3 The LVAP ion source and its infrastructure

In this chapter, the LVAP ion source commissioned in this work is described and its characteristics are explained. The setup of the ISTB at which the source is commissioned (figure 3.1), as well as the detection apparatus used for commissioning, is shown. The necessary trigger timings for operating the source are discussed.

3.1 Design criteria for the source setup

After commissioning the LVAP ion source, it will be operated at the 300 kV ion source platform of the CSR. Since the ion source platform is densely packed, the main design criteria for the LVAP ion source layout were size and portability. Between conducting experiments with different cluster species, the settings of the ion source need to be adjusted to the new target. For characterizing the new output, the source will be moved to the ISTB. A compact design, holding all ion source controls was thus necessary. This is achieved by mounting the LVAP ion source and its auxiliary equipments into a rack (chapter 3.3). A turbomolecular vacuum pump is used because of its small size yet high pumping speed.

3.2 The modified LVAP ion source

The disc-design, on which the LVAP ion source commissioned in this bachelor project is based, was originally developed by the Smalley group [20]. Characteristic for this design is a disc-shaped ablation target in contrast to the rod of target material used in other designs [17]. The design of the LVAP source commissioned in this thesis was recently developed in a collaboration between MPIK and Technische Universität Kaiserslautern. It is a modified version of the LVAP ion sources used by J. Meyer [2], J. Karthein [19] and C. Breitenfeldt et al. [9].

The main difference to the previous designs is an entirely redeveloped gas system (figure 3.3). A commercial cantilever piezo valve[1] is now used, allowing a variation of the gas pulse length in the range of 20 µs to 4000 µs. The previously used ceramic break has been removed, since mechanical forces applied to the gas system would quickly lead to damage of the break. The potential of the vacuum chamber housing the ion source (referred to as source chamber) is now separated from the potential of the ion source (referred to as source potential) using a PEEK insulator (figure 3.4). Unlike the previous versions, for this version the entire external gas system is placed on source potential. The gas line inside the source chamber has been replaced by a metal pipe helix. Because of its flexibility, this setup allows to easily vary the axial

[1] MassSpecpecD BV, ACPV2-300

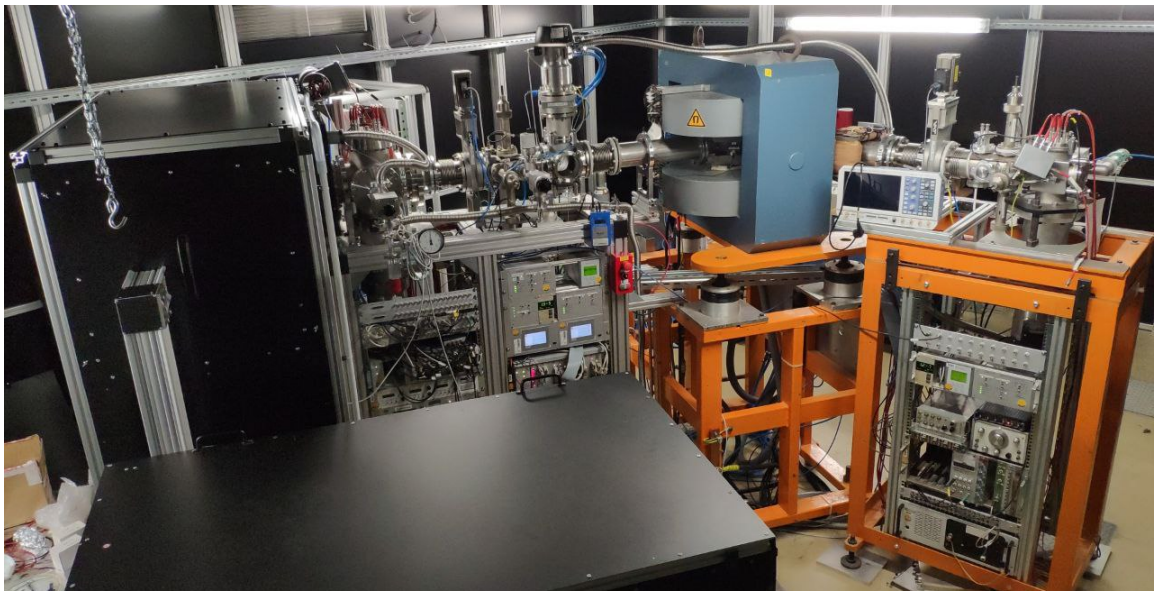

Figure 3.1: Photograph of the ion source rack housing the LVAP mounted at the ISTB. The rack can be seen on the left-hand side, behind the box in which the laser is placed.

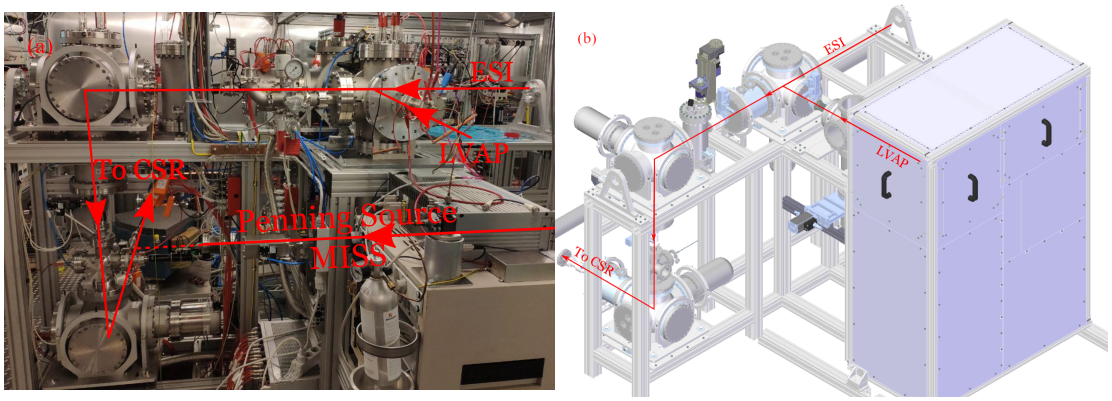

Figure 3.2: (a)Photograph of the 300 kV ion source platform. Onto the port where the LVAP ion source is foreseen, currently a Heinecken type Penning ion source is mounted. The other ion sources can not be seen in this picture. (b) Model of the LVAP ion source mounted to the 300 kV ion source platform. Red arrows indicate the ion trajectory.

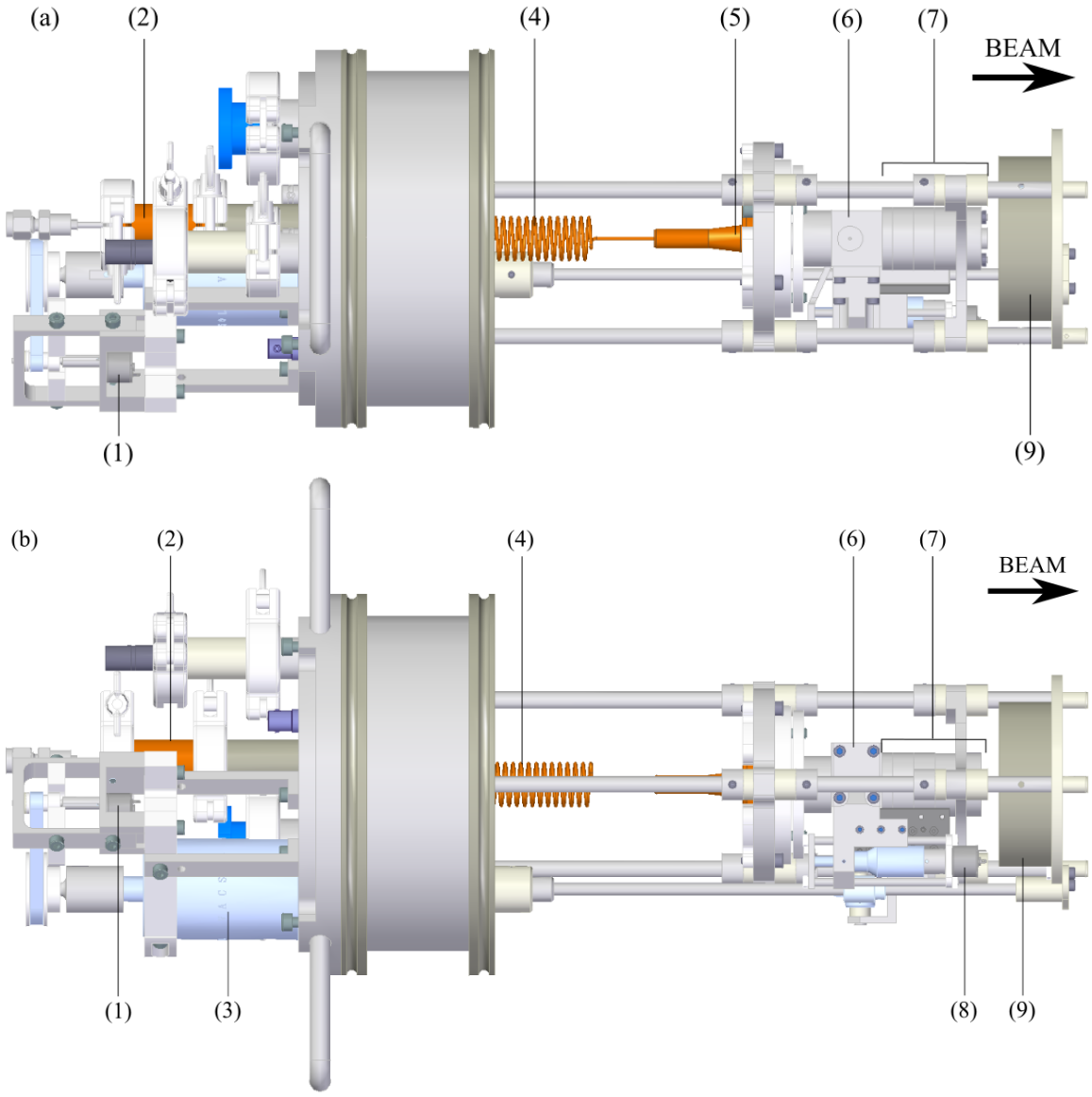

Figure 3.3: Setup of the LVAP ion source as seen from (a) the side and (b) below. The main differences to the previous versions are highlighted in orange. (1) motor for rotating the ablation target (2) PEEK insulator (3) rotary vacuum feed-through (4) metal pipe helix for expansion gas (5) cantilever piezo valve (6) vaporization block with ablation target inside (7) growth channel (8) inner motor for changing the trace on the ablation target (9) mesh

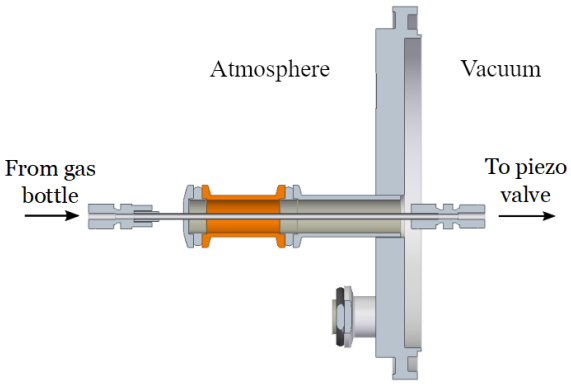

Figure 3.4: The new PEEK insulator which separates the potential of the source chamber from the source potential.

position of the source and therefore also the distance between growth channel and skimmer. These parameters can now be optimized for production of Al_4^- clusters.

3.2.1 Ablation target

A wide variety of cluster ions can be produced with an LVAP ion source [2]. The cluster constituents are determined by the material of the ablation target. The target itself is a thin round piece of foil with a thickness of 0.1 mm to 0.5 mm and a diameter of 12 mm. In order to produce Al_4^- clusters, a high-purity aluminium target[2] is used. It is glued[3] onto the target holder, which is mounted inside the source. In order to enable rotation of the ablation target, the holder is suspended with ball bearings. A motor[4] continuously rotates the target, and the laser therefore ablates a circular trace on the target. This motor is mounted outside the vacuum on the source flange to prevent overheating of the motor because of low heat transport inside the vacuum. It is connected to the target via a rotary vacuum feed-through and a worm gear. The idea was developed and first implemented in the work of J. Karthein [19]. To change the trace on the target, a second, identical motor is used for moving the target transversally to the laser beam. This setup is necessary to prevent the laser from hitting the same spot repeatedly, burning a crater into the target and impairing vaporization (compare section 2). The target can be changed without dismounting the source, preventing the necessity of realigning the laser beam after having changed the target.

[2]Sigma-Aldrich; 0.25 mm foil thickness, 99.999 % purity
[3]Torr Seal #9530001; epoxy glue suitable for high vacuum applications
[4]Faulhaber, 1512U012SR 324:1; 30 mN m

3.2.2 Ablation Laser

For target ablation, it is foreseen to use the second harmonic of a compact Q-switched Neodymium-doped Yttrium Aluminium Garnet (Nd:YAG) laser mounted onto the optical breadboard of the LVAP source rack. Since a suitable laser had been ordered but was not yet available at the time of the first experiments, a different Nd:YAG laser system[5] with similar output parameters was used. It was operated at a wavelength of 532 nm and a pulse repetition rate of 10 Hz. Each laser pulse has a duration of 4 ns to 6 ns and an energy of up to 100 mJ. The provisional laser system was too large to fit onto the breadboard. It was placed inside a separate box next to the LVAP source rack and the laser beam was transported to the ion source via several mirrors. About 10 % of the beam were decoupled using a beamsplitter[6] and used for measuring the laser power via an energy meter[7]. A convex lens with a focal length of 40 cm was used to focus the beam onto the ablation target through a 17 mm long channel with a diameter of 1 mm in the vaporization block (figure 3.3).

The beam intensity profile of the used Nd:YAG ablation laser follows approximately a Gaussian distribution. For a rough estimate of the power density after focusing the laser beam onto the target, the waist of the laser beam before passing the lens is assumed to coincide with the front focal plane of the lens [21]. The radius at the waist of the focused beam w_0' is then given by

$$w_0' = \frac{\lambda f}{\pi w_0} \tag{1}$$

where f is the focal length of the lens, λ the photon wavelength and w_0 its radius before focusing. The power density I_L of a laser pulse with energy E_{pulse} and duration t_{pulse} is given by

$$I_L = \frac{E_{pulse}}{t_{pulse}\pi w_0'^2} = \frac{E_{pulse}\pi w_0^2}{t_{pulse}\lambda^2 f^2}. \tag{2}$$

For typical values used in this experiment ($E_{pulse} = 1.6\,\mathrm{mJ}$, $t_{pulse} = 5\,\mathrm{ns}$, $w_0 = 5\,\mathrm{mm}$), one receives a power density on the order of $I_L \approx 10^{10}\,\mathrm{W\,cm^{-2}}$. Since the assumptions are not entirely correct, the actual power density is a bit lower but still beyond the ablation threshold for aluminium.

[5] EKSPLA, NL300 series
[6] Thorlabs, BSN10R
[7] Thorlabs, ES120C

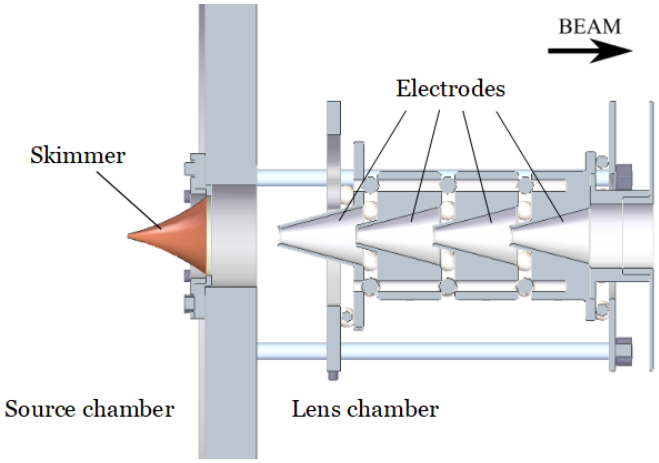

Figure 3.5: Cut through the skimmer and extraction system.

3.2.3 Gas system

To flush away the ablated target material and to enable cluster formation in the growth channel, short pulses of helium gas with a backing pressure up to 15 bar are used. The pulsed piezo valve is operated at 10 Hz repetition rate and a gas pulse length of 20 µs to 50 µs. It is used to reduce the gas load in the vacuum chambers. The modular design of the growth channel makes it very easy to vary the channel length in steps of 5 mm, simply by adding or removing some of the modules. The length of the growth channel is set to 45 mm by default with a diameter of 2 mm.

3.2.4 Electric potentials

Piezo valve, gas system and target are electrically insulated from the rest of the setup. Fiber-optic cables are being used for controlling the piezo valve. These parts can be placed on a common potential relative to the source chamber, using an external power supply. The source potential can be lifted up to ±50 V with respect to the potential of the source chamber. The source chamber itself is placed on a potential of ±5 kV and the ions leaving the source chamber through the skimmer are accelerated towards ground potential. A cylindrical mesh is mounted to the end of the source which can be set to a potential (referred to as mesh potential), to keep the ions centred.

3.2.5 Extraction

Extracting and accelerating gas phase ionic clusters can prove difficult because these procedures bear an increased risk of internal heating and fragmentation by collisions with residual gas particles [17, 12].

With a stepwise acceleration from a region with high residual gas density to a region with lower residual gas density, such collisions are minimized. The design of the extraction electrodes (figure 3.5 was developed by V. Schmidt, via simulation studies with conditions similar to those of an LVAP ion source [12]. Most of the ionic clusters produced in an LVAP ion source are in the centre of the beam, which is also its coldest part [17]. Before acceleration, a skimmer[8] with a 1 mm orifice is used to strip large parts of the buffer gas from the ion beam. Since the orifice of the skimmer is the only connection between source chamber and lens chamber, efficient differential pumping is possible, leading to vacuum pressures in the rest of the setup, several orders of magnitude better than in the source chamber. In chronological order in which the beam passes through them, the voltages used for extraction are 10 V, 100 V, 1000 V and 5000 V relative to the source chambers potential.

3.2.6 Trigger timings

The beam intensity of LVAP sources is strongly dependent on the relative timing between piezo valve and ablation laser [17]. Both operate at a frequency of 10 Hz, but with a small delay from laser trigger to piezo valve trigger, referred to as Piezo Delay (PD). Since ablation happens on a much faster time scale than gas flow, it should take place on the leading edge of the rising gas pulse [20], making the PD a negative value. Another important timing is the opening time of the valve, which controls the amount of buffer gas. It is specified at the driver unit of the valve and mainly important for cluster size and temperature, since more collisions with the buffer gas tend towards formation of larger clusters [17], but also towards higher cluster temperatures [22]. Due to its cavity design, the used ablation laser needs to be triggered and pumped by the flashlamp at exactly 20 Hz in order to prevent damage to the Nd:YAG-rod.[9] Via a frequency divider setting, the output frequency of the laser is set to 10 Hz. Another important parameter is the Q-switch delay of a laser, since it determines its output power. For the laser used in this work, the delay is set by the length of the trigger pulse. An overview of the relative timings is displayed in figure 3.6.

3.3 The ion source rack

Part of the initial design idea for the source setup is a compact design and high mobility of the source and its infrastructure, so it can be easily moved between ISTB and the ion source platform of the CSR. This is achieved by mounting the LVAP ion source and all controls into a rack (figure 3.7). The source chamber is placed on a mount that enables an easy alignment to the designated ion source port on

[8] Beam Dynamics, Inc., Model 2; Nickel
[9] Unstable laser cavity design for higher beam quality [23]

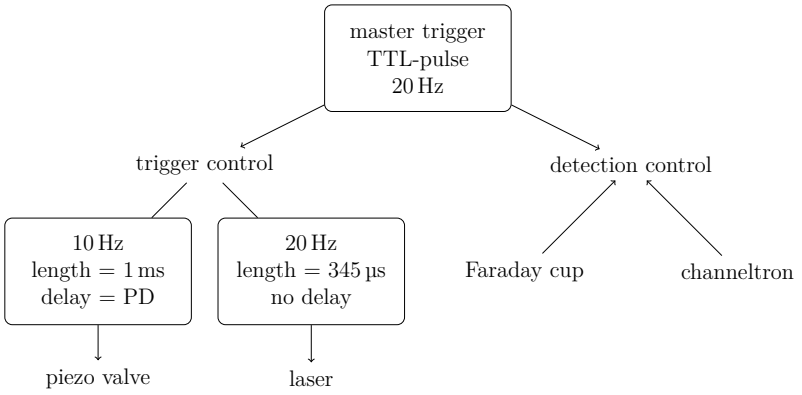

Figure 3.6: Overview of the relative trigger timings and trigger pulse lengths used in the experiments. Since the PD is a negative value, the valve is triggered before the laser. The Q-switch delay of the laser used in this work is set by the length of the laser trigger pulse.

the ion source platform. The mount is set on two rails, allowing it to be moved along the beam axis to make the extraction system accessible without the need to realign the source chamber. While the rack is mounted at the ISTB, it is placed on a substructure with variable feet. The source can then be aligned to the ISTB by adjusting the substructure while keeping the alignment to the ion source platform. The source chamber is pumped using a turbomolecular pump[10]. The source chamber and the frame holding the ion source controls are electrically insulated from the rest of the setup, since they will be lifted to a potential of $\pm 5\,\mathrm{kV}$ with respect to the ground potential. An optical breadboard is placed next to the source chamber. In addition to various optical components, a compact Nd:YAG ablation laser is foreseen to be mounted on the breadboard.

3.4 The Ion Source Test Bench

The ISTB is used for measuring the ion source output and determining the ion beam composition. It was developed by F. Nüßlein specifically for the purpose of testing new ion sources before operating them on the 300 kV ion source platform of the CSR facility[11]. The ISTB represents a magnetic mass spectrometer with a beam line length of approximately 3 m (figure 3.8). A 60° bending magnet is used for mass separation. In this chapter, a short description of the parts most relevant for this work is given.

[10] Pfeiffer, HiPace 700; $685\,\mathrm{l\,s^{-1}}$ pumping speed

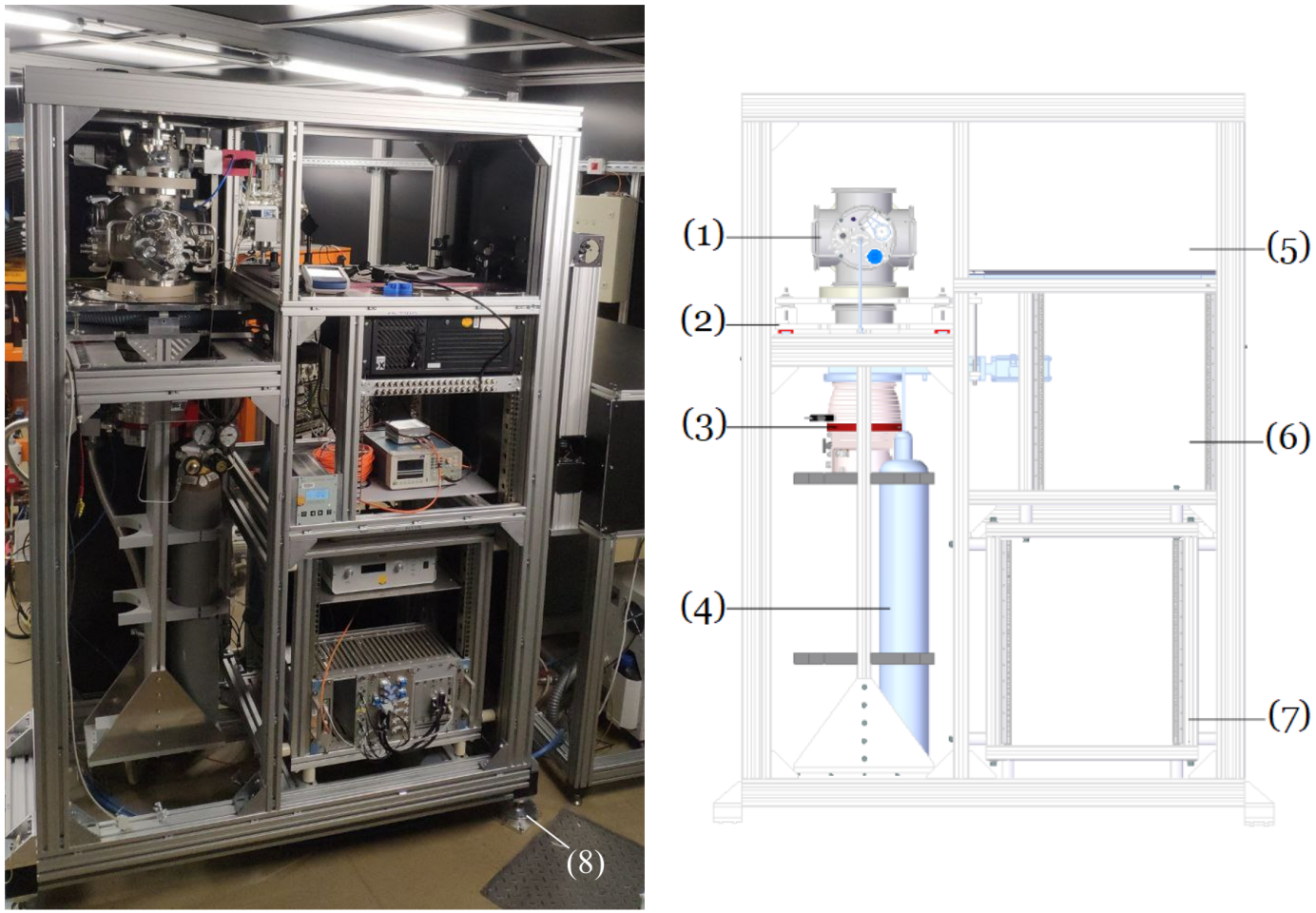

Figure 3.7: Rack housing the LVAP ion source without its covers. (1) source chamber (2) source chamber mount (3) vacuum pump (4) gas bottle (5) breadboard for laser setup (6) measurement controls (7) frame for ion source controls (8) substructure with variable feet

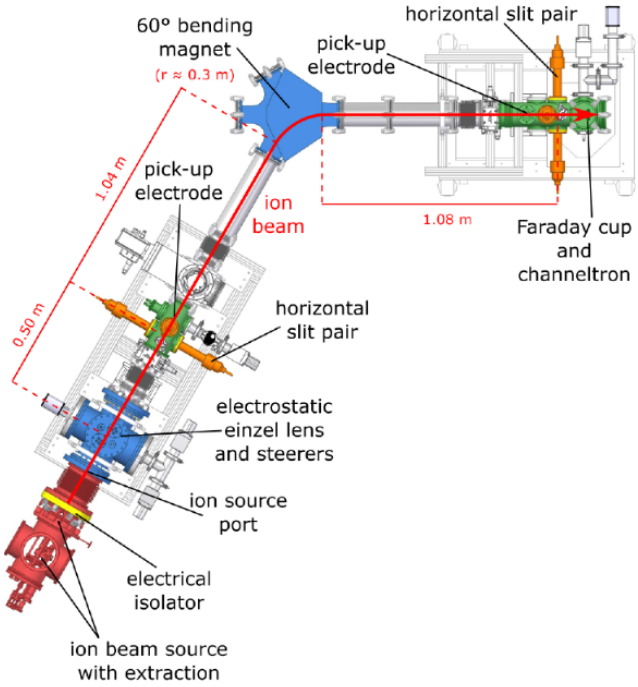

Figure 3.8: Bird's-eye view of the ISTB. Taken from [11].

3.4.1 Ion optical elements

Several ion-optical elements are mounted in the ISTB for optimal beam transport. They were described in detail in [11]. Before progressing through the bending magnet, the ion beam passes through an electrostatic einzel lens and two horizontal and vertical steerer pairs. The einzel lens serves to focus the beam, while the steerer pairs allow for correcting the ion beam offset in x-direction and y-direction respectively.

The resolution of the mass spectrometer is determined by the opening width of the second horizontal slit pair. It is placed in the focal point of the ion beam behind the bending magnet. While a smaller setting of the slit opening gives a better resolution, it also blocks a higher fraction of the incoming beam and reduces the overall ion signal, making it more difficult to detect small ion currents.

3.4.2 Ion detection

For detection of a broad range of currents, a setup combining a Faraday cup and a channeltron is used (figure 3.9). Ions entering the detector system produce electrons through secondary electron emission when hitting the wall of the detector. In the Faraday cup mode, the ion beam current is measured at the cup electrode of the detector with a nanoamperemeter. The charged repeller electrodes prevent secondary

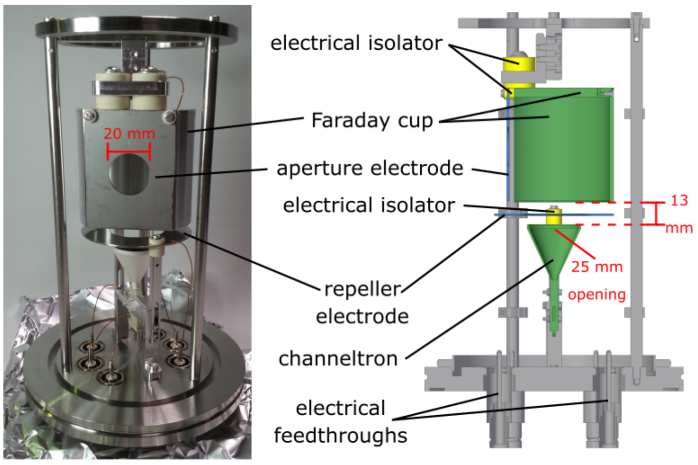

Figure 3.9: Detector system of the ISTB. Taken from [11].

electrons from escaping the detector and falsifying the measured signal. With this mode, ion currents down to 10 pA can be measured. In the channeltron mode, the cup electrode is still hit by the incoming ions, but used as a converter plate. For each incoming ion, the emitted electrons are accelerated into the cone of the channeltron. Repeated collisions of the electrons with the lead glass wall of the cone trigger an electron avalanche by secondary electron emission. The electron avalanche is then collected at the anode at the bottom of the cone and converted into a characteristic voltage pulse, which can be counted with suitable electronics. The channeltron is able to detect single ions at a rate up to $10^7\,\mathrm{s}^{-1}$, corresponding to 1.6 pA [11].

4 Commissioning an LVAP ion source

The performance of an LVAP source depends on many variables. Determining good values for these variables is non-trivial, since they are different for each source design and often dependent on each other [17]. In the first part of this chapter, the most important tests and alignment steps for ensuring the proper functionality of the setup is briefly shown. In the second part, a roadmap for optimizing the variables for obtaining a maximum Al_4^- yield is developed.

Over the curse of this bachelor thesis, an LVAP ion source was assembled and the infrastructure necessary for operating the source was set up. Ion source and auxiliary equipment were taken in operation and the functionality of the equipment was tested. In the commissioning process, the first practical step is the determination of the PD. Unfortunately after performing these measurements, technical problems occurred inside the commercial cantilever piezo valve. Since the valve would not open or close again, it had to be sent in for repair. It was not sent back by the manufacturer in time for carrying out the other measurements foreseen along the Al_4^- roadmap.

4.1 Necessary tests and alignment steps prior to commissioning

Aligning the ion source

To ensure proper operation of the magnetic mass spectrometer setup, the ion beam has to propagate along the axis defined by the position and orientation of the bending magnet. Therefore, the source chamber, and most importantly the extraction, were aligned accordingly. The optical axis of a Taylor-Hobson telescope was aligned to the ion beam axis of the ISTB, without the source being mounted into the experiment, analogously to the alignment process performed by F. Nüsslein [11]. A bull's-eye target was placed at the position of the skimmer. Source chamber and extraction, which are mounted on rails, were simultaneously pushed towards the lens chamber of the ISTB until the source chamber flange touched the ion source port. This position is the final position at which the source is later operated. Using the target and the first electrode of the extraction system as reference points, source chamber and extraction were aligned to the optical axis of the telescope. It is verified that all four electrodes are placed concentrically with the beam axis. It is also verified, that after the alignment process the flanges of the extraction chamber and the lens chamber still well fit together mechanically. Inside the source chamber, the inner part of the ion source is automatically centred by the intrinsic mechanical fixation points of the three guiding rods which ensure that expansion channel and skimmer are placed concentrically.

Testing the vacuum of source chamber and lens chamber

The ion source is housed inside a separate vacuum chamber, which is pumped by a dedicated turbomolecular pump. Between source chamber and lens chamber, a skimmer is mounted. During operation, the small orifice of the skimmer is the only connection between source and lens chamber, allowing for efficient differential pumping. After pumping the experiment for over 72 h, a vacuum pressure of 4×10^{-7} mbar was measured in the source chamber. In the lens chamber, a vacuum of 5×10^{-8} mbar was achieved. The difference between these pressures is probably due to copper gaskets being used in the lens chamber, contrary to standard O-rings used for the source chamber. When operating the piezo valve and the gas inlet at the intended settings (11 bar absolute pressure, 10 Hz repetition rate, 50 µs opening time, 200 V piezo holding voltage), vacuum pressures of 3×10^{-5} mbar and 8×10^{-8} mbar were measured in the source and lens chambers respectively.

Checking proper insulation of elements on high voltage

Proper electrical insulation of source chamber and extraction are very important for preventing undesired electrical breakdowns. High voltage tests at up to ±5.5 kV were performed using an insulation tester[11] while all other parts were grounded. The voltage was increased stepwise and then held at the voltage of interest for at least 2 min. At first, the tests were performed in a vacuum on the order of 10^{-7} mbar without a helium gas load. Electrode 1 and 2 of the extraction were tested at ±0.5 kV, where resistances above 1.5 TΩ were measured. Electrode 3 and 4 were tested at ±5.5 kV, showing resistances of 2.7 TΩ and higher. The source chamber was tested at ±5.5 kV as-well, showing a resistance of 66 GΩ. Afterwards, electrode 3 and 4 were tested again with a helium gas load, at a vacuum pressure of 2×10^{-6} mbar at ±5.1 kV, showing a resistance of 30 GΩ and higher. The measured resistances are high enough to ensure that no high-voltage breakdowns will occur during operation, on condition that the voltage is increased stepwise.

Testing the motor rotating the target

Two motors are in use for a continuous target movement, preventing loss in ion output from repeated ablation of the same spot (chapter 3.2). Since the motor mounted outside the vacuum on the flange is continuously running, it is particularly susceptible to malfunction. The constancy of its revolution time was tested to ensure that the motor provides constant torque over long running times. The revolution time of the gear belt, connecting the outer motor to the rotatory feed-through, was measured over the course of 16 h. Since it increased from (46 ± 2) s to (50 ± 2) s, the motor is

[11] Megger, S1-1568; 15 kV maximum test voltage

not strong enough for permanent operation. Hence it was replaced by a motor with higher permanent torque[12]. The measurement was repeated and revolution times of (52 ± 2) s and (51 ± 2) s were measured, before and after the motor running for 16 h respectively. The new motor is thus suitable for rotating the target over long running times.

Aligning the laser for target ablation

For ablation, the laser beam needs to be focused onto the surface of the target. It enters the ion source through a channel in the vaporization block of 17 mm length and 1 mm diameter. To align the laser beam with the channel in the vaporization block, two rods of different length with bull's-eye targets on their ends were alternately mounted onto the outside of the vaporization block (figure 4.1 (a)). By adjusting the laser beam to the bull's-eye targets in an iterative manner, the beam could pass through the channel in the vaporization block and hit the ablation target. To make sure the beam proceeds through the channel and does not scatter off its wall, the target was dismounted. Without the target being mounted, the beam could pass through the source and was observed behind the source. After remounting the target, by increasing the power of the laser beyond the ablation threshold, it was made sure that the target is in the focus of the beam. A distinct noise can be heard when ablation takes place. The proper alignment was then double checked by inspecting the aluminium target after ablation (figure 4.1 (b)).

4.2 Roadmap for commissioning the LVAP ion source

The main part of the commissioning process consists of finding the optimal settings for the parameters determining the performance of an LVAP ion source (figure 3.3). A series of measurements is required, with each measurement optimizing a different parameter, pursuing the goal of maximum Al_4^- yield. In the this chapter, a roadmap of measurements necessary for determining these parameters is presented and motivated.

Many of the parameters depend on one another, therefore the roadmap must be seen as an iterative process, with steps being repeated several times with different settings. The first step of each iteration is setting the growth channel length (step **Length of the growth channel** below) and position since these mechanical modifications are very time consuming. The source needs to be dismounted every time, consequently the source chamber has to be vented and the laser needs to be realigned afterwards.

[12] Faulhaber, 2619S012S R 207:1; 100 mN m

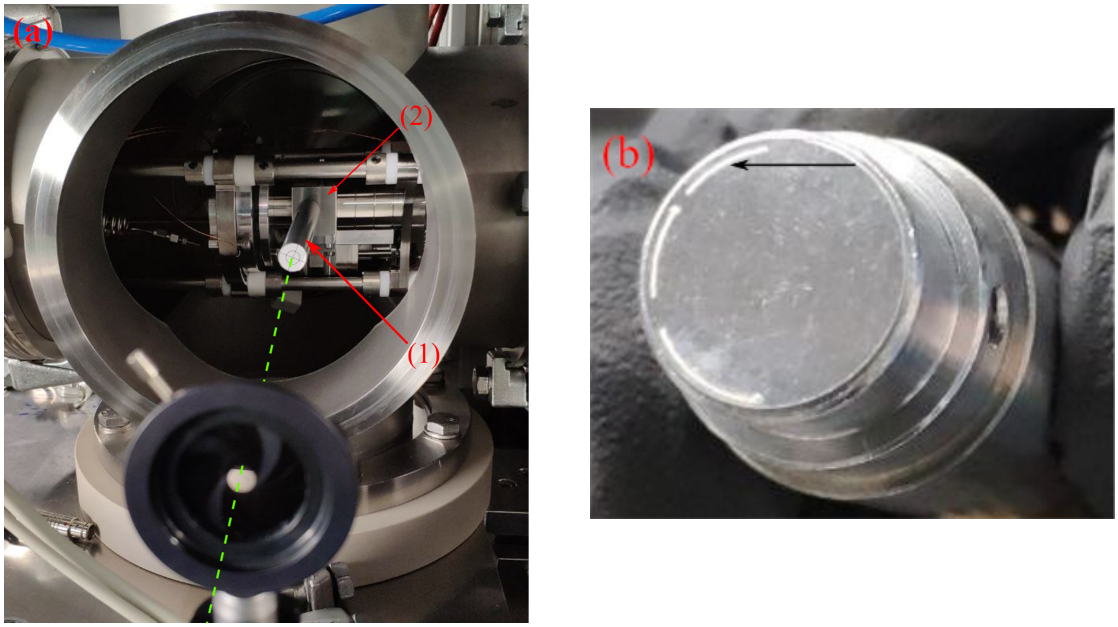

Figure 4.1: (a) Photograph taken during the laser beam alignment. The green dashed line represents the laser beam. (1) rod with bull's-eye target on its end (2) vaporization block. For details of the alignment process see text.
(b) Aluminium target after ablation. The round light grey trace near the outer edge of the target results from ablation. The trace is interrupted where the laser was switched off.

Piezo delay

The delay between laser pulse and gas pulse, the so-called Piezo Delay (PD), is one of the most crucial settings when commissioning an LVAP ion source. If it is off by only tens of microseconds, the gas pulse cannot fulfil its function of carrying the ions produced by the laser pulse on the target surface toward the skimmer, hence the ions will not be ejected from the source and move towards the skimmer. In this first measurement, it is verified whether ions are transported to the skimmer and which PD maximizes the number of ions arriving at the source exit.

The ions are not extracted from the source chamber, since no voltages are applied to source, source chamber and extraction electrodes. The measurement was performed via a digital oscilloscope[13] and a low noise current amplifier[14] connected to the skimmer (figure 4.2). The plasma produced by ablation of an aluminium target with a pulsed laser (10 Hz, 5 ns FWHM) is flushed out of the source and onto the skimmer by the helium gas pulse. There, the induced current is measured. Since only the net current was measured, there was no information obtained what ion species were produced in the source. About 10 % of the laser beam are decoupled and detected using a photo diode[15]. The laser signal's rising edge was used as zero point for the measurement. The measurement was repeated for different PD settings to find the setting with the highest signal yield.

Measurements for this step could be carried out and their results will be described in chapter 5. Since after the measurements the piezo valve malfunctioned, the following steps could not be carried out.

Ion extraction and voltages of the ion optics

Before meaningful mass spectra of the ion beam can be measured, it is necessary to adjust the voltages of the electrostatic ion optics of the ISTB (chapter 3.4.1). In this measurement, by extracting anions from the source, it is verified whether the ion extraction system is working, and the ISTB is prepared for conducting quantitative measurements of the mass selected ion current. The source is operated as intended and with extraction voltages applied to the electrodes (chapter 3.2.5). Whether ions are extracted from the source can be determined by looking for an ion signal at the horizontal slit pair before the bending magnet. By variation of steerer voltages and the magnetic field at the ISTB, an ion signal is then searched using the Faraday cup behind the magnet. The ion optics, namely steerers and einzel lens, are adjusted for

[13] Pico Technology, PicoScope 5444D; 200 MHz bandwidth
[14] FEMTO, DLPCA-200; 500 kHz bandwidth, 900 ns rise/fall time (10 %-90 %), 10^5 V/A gain
[15] Thorlabs, DET10A2; 1 ns rise time

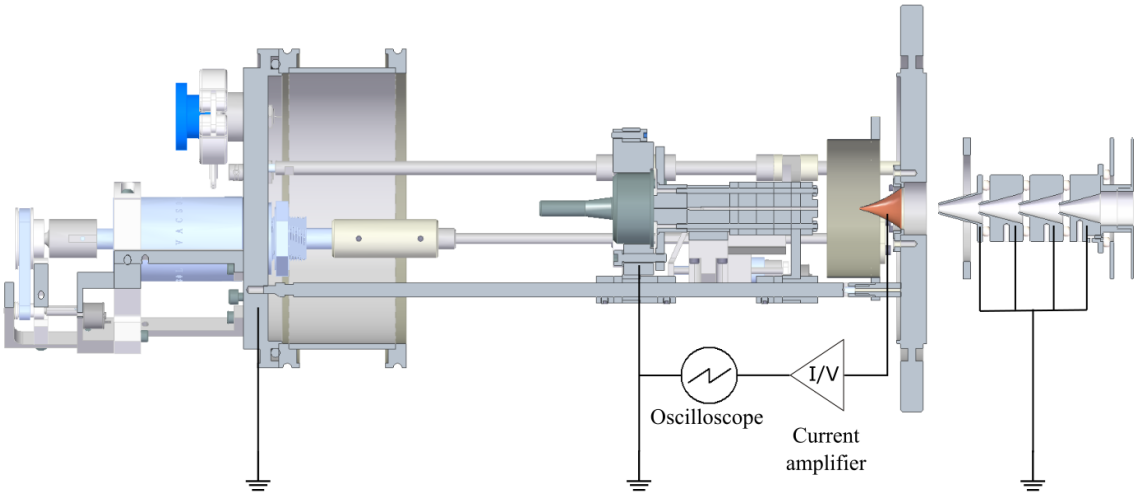

Figure 4.2: Electrical circuitry for measuring the PD without extraction from the source chamber. All parts are grounded except for the skimmer, to which an oscilloscope is connected via a current amplifier.

obtaining a maximum signal.

If no ions are extracted from the source, the position of the growth channel is adjusted. An incorrectly set distance between growth channel and skimmer might cause beam gas to scatter off the skimmer and induce turbulences that block the beam from passing through the orifice (step **Gas pulse** below).

Length of the growth channel

After successfully conducting the steps mentioned above, the roadmap continues in an iterative manner. First step of every iteration is setting the growth channels length, by adding or removing modules from the setup (chapter 3.2.3). The other parameters are then optimized for each growth channel length. The relative abundance of different cluster sizes is strongly correlated to the length of the growth channel. A longer growth channel favours the formation of bigger clusters, since it gives more time for cluster formation.

Position of the growth channel

As noted above, the distance between skimmer and nozzle of the growth channel can have a strong influence on the beam output. Turbulences from beam gas scattering off the skimmer can block the beam from passing through the orifice of the skimmer

if the distance between nozzle and skimmer is too short [17]. If the distance is set too large, the beam might broaden too much during supersonic expansion of the carrier gas and less clusters pass through the orifice of the skimmer.

Laser power

The ablation laser's pulse energy is the most critical variable in the performance of an LVAP source [17]. A higher power density leads to more target ablation, but the higher density of the ignited plasma also leads to more absorption, heating the plasma further and therefore possibly leading to the production of fewer clusters [17, 22]. It also leads to a faster consumption of the target and more unwanted redeposition of ablated material inside the source. In this measurement, the power of the nanosecond pulsed laser is optimized for a maximum output of Al_4^- anions. The measured laser power with the highest yield is expected to be found in the range of 10 mJ to 25 mJ per pulse [22].

Turning speed of the target

Continuous rotation of the ablation target is important for a stable ion output. If the ablation laser repeatedly hits a single spot on the target, a crater is burned into the target and the ignition of plasma is impaired [17]. A motor is mounted outside the vacuum chamber and connected to the target via a rotational vacuum feed-through for constant target rotation. The turning speed must be adjusted so that the target is ablated evenly and an uniform shot-to-shot signal is obtained. Eventually, the trace from target ablation becomes too deep and needs to be switched. The optimal turning speed of a target is mainly dependent on target material and laser power.

The setup is ready for recording meaningful mass spectra only after adapting the turning speed of the ablation target to the laser power.

Gas pulse

During expansion, collisions with the expansion gas are necessary for cluster formation and cluster cooling. A bigger gas load leads to more collisions between expansion gas and ionic clusters, and therefore to more efficient collisional cooling [17]. Despite the skimmer separating most of the expansion gas from the ion beam, a fraction of the gas still enters the lens chamber downstream. Inside the lens chamber, the ions are accelerated electrically by the extraction through the residual expansion gas. Collisions with the gas atoms excite the internal rovibrational states of the anionic clusters and might lead to fragmentation of the cluster [19]. By using a stepwise acceleration with four electrodes, these effects are reduced, but not negligible

(chapter 3.2.5). With a higher gas load, the impact of these effects increases. In this measurement, absolute backing pressure of the helium expansion gas and opening time of the piezo valve are optimized for a maximum Al_4^- yield.

Mesh potential and source potential

Downstream of the growth channel, a cylindrical mesh is mounted to which a voltage can be applied. The mesh potential is for focusing the ion beam before it passes through the skimmer, reducing the loss of anionic clusters during extraction. But by applying external electrical fields to the dense ion beam, charge separation occurs and space charge effects become an issue. These effects lead to a decrease in overall beam density. With a high expansion gas density, applying external electrical fields is particularly problematic before passing through the skimmer, since they induce substantial turbulences leading to internal heating of the ions. [17]

For a previous version of the LVAP ion source, cluster output was found to be dependent on the voltage applied to the source [2]. By variation of the source potential, it is checked whether this dependency still exists with the new extraction, and if it does, what potential gives the highest Al_4^- yield.

5 Data analysis

The current induced at the skimmer was measured for different PD settings. The design of the measurement is discussed in chapter 4.2. After laser ablation from the target, the induced plasma is flushed from the vaporization block towards the skimmer by the gas pulse. Charged particles passing through the skimmer orifice or hitting onto the skimmer induce a current onto the skimmer. When passing through the skimmers orifice, the signal induced by a bunch of charged particles consists of two peaks: For positively charged particles, a positive current when entering and later a negative current when exiting the skimmer is induced and vice versa. The time between the two signals is given by the temporal length of the particle bunch. When hitting onto the skimmer, the charged particles may induce a charge corresponding to their polarity through charge transfer. Even though additional effects, such as charged particles knocking electrons out of the skimmer (secondary electron emission), make it impossible to determine the exact ion number, a lot can be learned from this measurement. In this chapter, first an interpretation of the observed timetrace is given. Afterwards, the data is analysed under the particular viewpoint of the PD for optimal signal yield.

During all measurements, an absolute backing pressure of 5 bar was set for the helium pulse. The laser energy was set to 1.3 mJ per pulse, as measured using a power meter. Without gas being pulsed into the source chamber, a vacuum of 4×10^{-7} mbar was measured. Observing the signal triggered by the laser pulse for times up to 150 µs, the PD was varied in the range of −200 µs to +100 µs in steps of 10 µs (figure 5.1). In the observed timetraces, a signal could only be observed for a PD between −110 µs to −90 µs, with the signal for a PD of −110 µs being very weak. This range was scanned again in smaller steps of 1 µs.

In the observed timetraces (figure 5.1), approximately 300 ns after the photo diode signal, a strong negative peak is seen, with two smaller positive peaks right before and after. Another, stronger and much broader positive peak is observed with its maximum around 106 µs. Looking closer at the electron signal (figure 5.1 (c)), for the strong negative peak, a fall time (10 %-90 %) of almost 150 ns and a rise time of 500 ns can be determined. For the small positive peak before the negative peak, an even smaller rise time can be seen. These rise and fall times are far below the specified time resolution of the current amplifier, as observed for previous measurements [11].

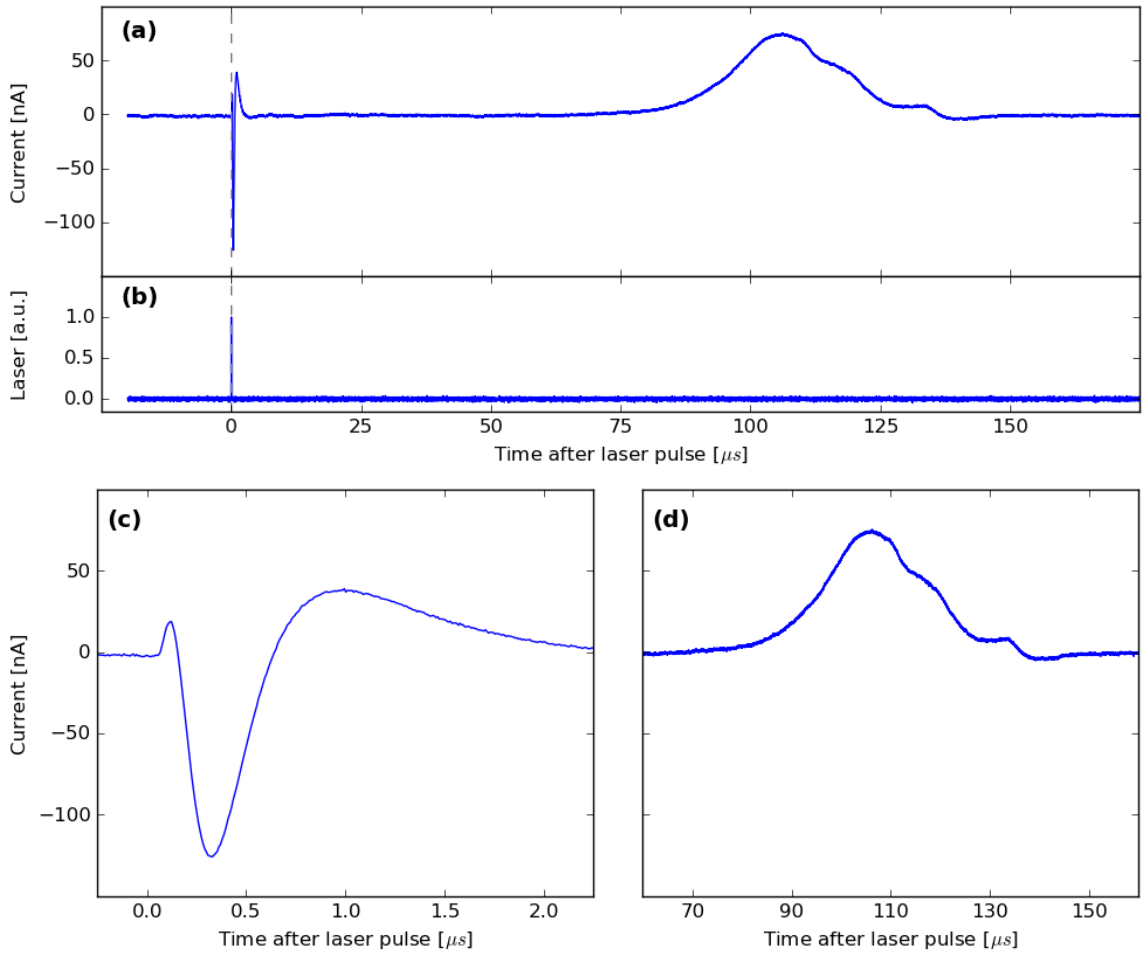

Figure 5.1: Typical measurement of the skimmer current (single waveform, no averaging). (a) Timetrace of the skimmer current showing an electronic signal at around 1 µs and a broader ionic signal at around 100 µs. (b) Signal of the laser pulse, detected with a photo diode. (c) and (d) Zoom in on the electronic and ionic signal respectively. PD=−98 µs

5.1 Timetrace interpretation

5.1.1 The electron signal

The earliest strong peak seen in the observed timetrace is of negative polarity and its early timing implies a high velocity of the inducing charged particles. These findings suggest that it is not induced by ions but fast electrons. This assumption is motivated by average ion velocities on the order of $10^4\,\mathrm{m\,s^{-1}}$ and average electron velocities on the order of $10^7\,\mathrm{m\,s^{-1}}$ observed by Margarone et al., after ablation of copper and tantalum with nanosecond laser pulses [24]. From dividing the distance $d = (110 \pm 5)\,\mathrm{mm}$ between target and skimmer by the time of the peak $t_e = (0.32 \pm 0.26)\,\mu\mathrm{s}$, one obtains a lower boundary of the electron velocity $v_e = (3.4 \pm 2.8) \times 10^5\,\mathrm{m\,s^{-1}}$. The given uncertainty is estimated from the peak width. The estimated velocity only serves as a lower boundary since the electrons are emitted perpendicular to the direction of the growth channel during ablation. Therefore, they undergo many collisions with the growth channel on their way towards the skimmer, resulting in a much longer effective travel distance.

A zoomed-in view of the electronic signal can be seen in figure 5.1(c). The observed form suggests a superposition of two signals, as discussed at the beginning of this chapter: a rather simple negative peak induced by charge transfer of electrons hitting the skimmer and a second signal, induced by electrons travelling through the skimmer orifice. Since the electron pulse is only a couple of nanoseconds long, these two peaks are very close together, with the negative peak having about the same timing as the signal induced by electrons hitting the skimmer. The combination of these effects fit the observed negative and following positive peak very well.

Looking at the first positive peak implies that for the earliest electrons, which are those with the highest energy, secondary electron emission dominates the signal. When one of these fast electrons hit the nickel skimmer, it can excite a valence electron of the skimmer until it escapes [25]. Assuming an average energy of the primary electron on the order of $10^2\,\mathrm{eV}$ to $10^3\,\mathrm{eV}$, as determined previously by Margarone et al. for copper and tantalum [24], the electron energies exceed the emission threshold and lie in a regime of high secondary electron yield for nickel [25]. When both primary electron and secondary electron are not detected, a net positive charge is induced.

5.1.2 The ionic signal

Looking at the observed timetrace, the later, broader and positive peak looks like three closely overlapping peaks, as can be seen in figure 5.1(d). It is induced by ions from the plasma, and ionic clusters formed during expansion in the growth channel. The polarity of the peak polarity indicates a strong surplus of positive ions, which

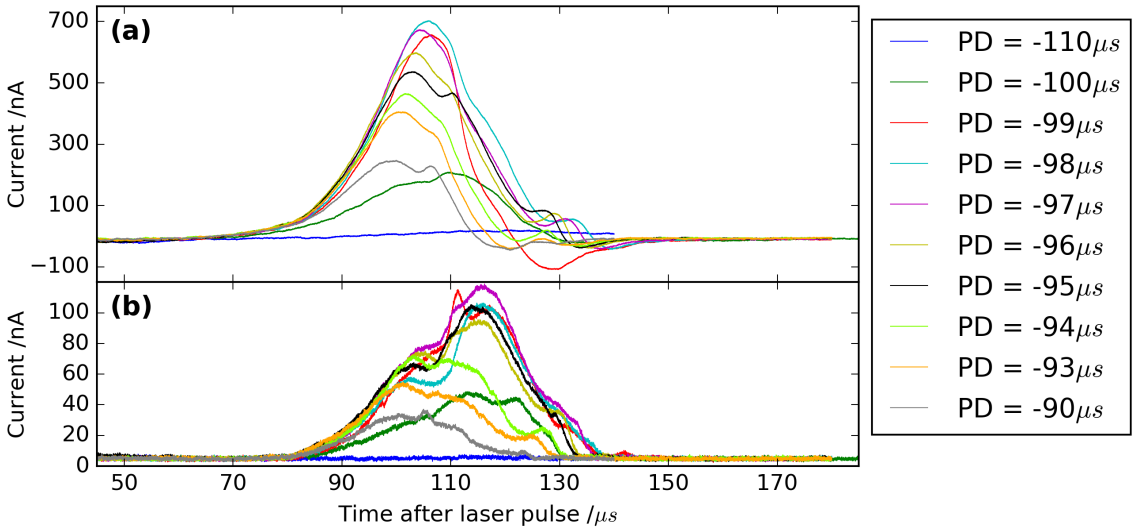

Figure 5.2: a) Averaged ionic signal and b) corresponding standard deviation of 32 measurements for each of the 10 different PD values.

is not surprising since ablation produces a plasma mainly consisting of neutral and cationic aluminium atoms [17].

The measurements for a PD of $-110\,\mu s$ will not be taken into consideration from now on, except stated otherwise, since they do not show the same ionic peak and only serve as a reference for very low signals. In figure 5.2, the averaged ionic signal is plotted for each PD. All measurements show the same three peak pattern for the ionic signal with different relative intensities. For some settings, the third peak is of negative polarity. Positive ions travelling through the skimmers orifice induce first a positive and later a negative pulse, as discussed at the beginning of this chapter. This effect might be the cause for the negative peak. Another possible explanation is a surplus of anions at the end of the ionic signal. Further measurements, also considering the relative abundance of anions and cations for different PDs, would be necessary to determine the most likely cause.

In figure 5.3, in which the average timing of the maximum current is plotted against the PD, a strong correlation between the two variables can be seen. A linear function $ax + b$ is fitted to the data between PD$=-99\,\mu s$ and PD$=-93\,\mu s$. The data point at $-100\,\mu s$ is not taken into account when fitting, since its maximum is at the second peak, whereas all other maxima are at the first peak. The data point at $-90\,\mu s$ is also not considered, since the maximum is shifted to the end of the first peak. From the linear fit, a slope of $a = -0.96 \pm 0.05$ was determined, with a re-

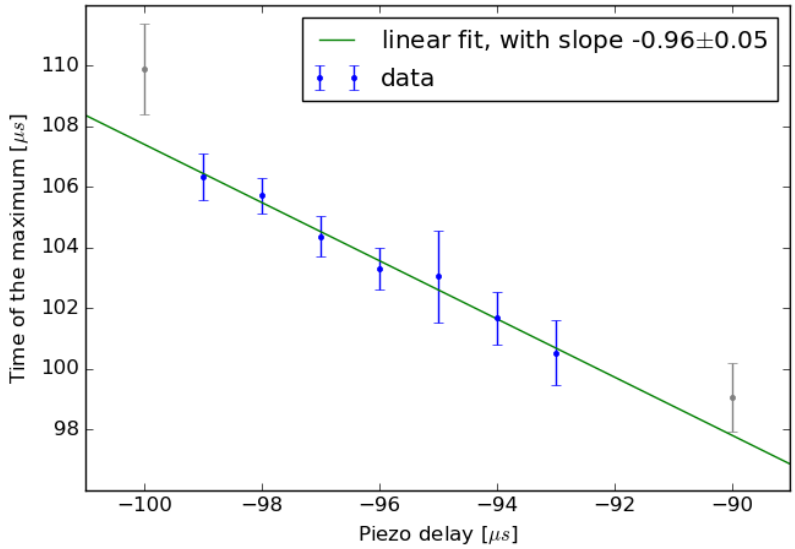

Figure 5.3: Average time of the maximum for each PD. The error is given by the standard deviation of the average. A linear function (green) is fitted to the data between PD=−99 µs and PD=−93 µs (blue).

duced chi-squared value of $\chi^2_{red} = 0.10$, which corresponds to a fit probability of 99 %.

This correlation of approximately $a = 1$ makes it evident that the timing of the ionic signal is determined by the timing of the gas pulse. This finding also confirms that the ionic signal is induced by ions from the ablation plasma being flushed to the skimmer.

In figure 5.3 and for all further calculations, the standard deviation of the average is used as measure of the statistical uncertainty. This is motivated by the observation that the distribution of the relative deviation from the averaged waveform follows a Gaussian profile, as can be seen in figure 5.4. A Gaussian function is fitted to the data, giving a mean value of $\mu = 1.0$ and a standard deviation of $\sigma = 0.13$.

5.2 Piezo delay for optimal signal yield

When changing the relative timing between laser pulse and gas pulse, different states of the ablation plasma are flushed out of the source. Meaning, by varying the PD, the plasma is probed in its different stages. The main goal of this measurement is to determine the PD for which the most ions are flushed out of the source. Ideally, by integrating over the measured current, the net charge is determined, and by integrating over the absolute value of the current, the total ion yield is determined.

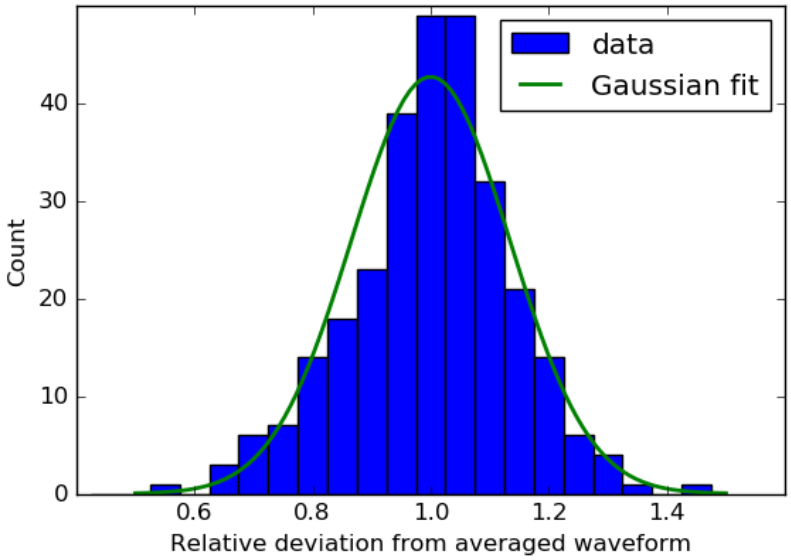

Figure 5.4: Histogram of the relative deviation from the averaged timetrace, at t=105.9 µs after the laser pulse. Plotted for all PDs. Green: Gaussian function with $\mu = 1.0$, $\sigma = 0.13$.

The measured ionic pulse contains both positive and negative ions, and the signal is created by different effects, which partially cancel each other out. Therefore, to prevent a false sense of knowing the absolute number of ions being produced, the integral over the absolute value of the waveforms will not be referred to as total ion yield but signal yield.

In figure 5.5, the average integral over the absolute values of the current is plotted for each PD. A very steep rise can be seen around PD=−100 µs towards a maximum at PD=−98 µs. The estimated values descend slowly to 37 % of the maximum value, at PD=−90 µs. A smaller PD corresponds to a longer time between gas pulse and laser pulse. From figure 5.5, it can be seen that if this time is too long (PD is too small), the plasma is created after the maximum of the gas pulse and the ions will not be extracted from the source. If the plasma is created too long before the gas pulse, the ions will only partially be extracted, with some of the material likely redepositing inside the source. Since the highest value was calculated for PD=−98 µs, this is probably the optimal setting for highest signal yield.

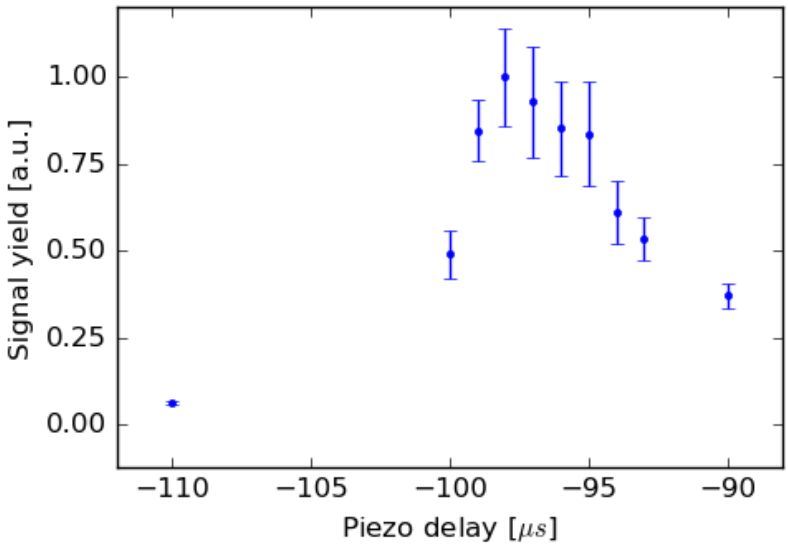

Figure 5.5: Average of the integral over the absolute value of the current for each PD.

6 Conclusion and outlook

Over the course of this bachelor project, a new LVAP ion source for production of cold Al_4^- clusters was taken into operation. The ion source and its auxiliary equipment were assembled and set up at the ISTB. All necessary tests and alignment steps were successfully performed (chapter 4.1). A roadmap of measurements required for commissioning the LVAP ion source was developed (chapter 4.2). Unfortunately, only the first step of the commissioning process could be conducted, since internal technical problems occurred in the commercial piezo valve.

It could be verified that ions are indeed produced in the LVAP ion source and that they are ejected from the source by a gas pulse (chapter 5.2), as foreseen in the LVAP concept. The output of the ion source, consisting of an early electron signal and an ionic signal, was well understood (figure 5.1). It was seen that short ion pulses with a length of about 25 µs are produced by the source (figure 5.2). The measured ion output current was found to be rather stable in time, where its intensity fluctuations roughly follow a Gaussian distribution (figure 5.4). It could also be seen that the timing of the ions ejected from the source is determined by the timing of the expansion gas pulse (figure 5.3). After changing the gas pulse timing, one therefore only needs to adjust the measurement timings by the same amount. These findings indicate that the LVAP ion source is suitable for future experiments.

It was found that the piezo valve must be opened about 98 µs before the laser pulse (PD=−98 µs) for the gas pulse to carry the optimal amount of any ions towards the skimmer behind the ion source. Future measurements will have to clarify whether this PD is also the optimal setting for a maximum Al_4^- yield. Following the extraction of ions from the source, the next steps foreseen in the roadmap will be performed (chapter 4.2). The ISTB will be tuned to the LVAP ion source, by setting the voltages of the ion optics. In an iterative process, the optimal settings for a maximum Al_4^- output will be determined. Since the parameters strongly depend on each other, the measurements need to be repeated for different growth channel lengths and positions. Beginning with the most important variables, laser power and gas pulse will be optimized. Optimal turning speed of the ablation target will be determined and it will be checked whether setting a source potential and mesh potential improves the output.

After optimizing the LVAP ion source for a high enough Al_4^- yield, it should fulfil all requirements for conducting meaningful experiments at the CSR. It could then be transported to the 300 kV ion source platform of the CSR. Measurements of the cooling processes of Al_4^- in even lower rovibrational states will then come into reach.

List of Figures

1.1 Schematic overview of the CSR 2
2.1 Schematic overview of an LVAP source. 5
3.1 LVAP mounted at the ISTB 7
3.2 Ion source platform (300 kV) 7
3.3 LVAP ion source. 8
3.4 Cut through the new PEEK insulator. 9
3.5 Extraction system with skimmer 11
3.6 Trigger timings and trigger pulse lengths. 13
3.7 Rack housing the LVAP ion source 14
3.8 Overview of the ISTB 15
3.9 Detector system of the ISTB 16
4.1 Photographs taken during the laser beam alignment 20
4.2 Electrical circuitry during PD measurement. 22
5.1 Typical timetrace as seen on the oscilloscope. 26
5.2 Ionic peak for different PDs 28
5.3 Timing of the maximum for each PD 29
5.4 Histogram of the relative deviation for all PDs 30
5.5 Integral over the current for each PD 31

References

[1] R. L. Johnston. *Atomic and molecular clusters*. CRC Press, 2002.

[2] J. Meyer. "Inbetriebnahme einer Laserverdampfungsquelle mit „Pick-Up "Einheit & Reaktionen kationischer Tantalcluster mit kleinen Kohlenwasserstoffen". Diploma Thesis. 2009.

[3] E. Campbell and R. Levine. "Delayed ionization and fragmentation en route to thermionic emission: Statistics and dynamics". In: *Annual review of physical chemistry* 51.1 (2000), pp. 65–98.

[4] O. Aviv, Y. Toker, D. Strasser, M. Rappaport, O. Heber, D. Schwalm, and D. Zajfman. "Competition between delayed ionization and fragmentation of laser-excited Al 4-". In: *Physical Review A* 83.2 (2011), p. 023201.

[5] H. Zettergren, A. Domaracka, T. Schlathölter, P. Bolognesi, S. Díaz-Tendero, M. Łabuda, S. Tosic, S. Maclot, P. Johnsson, A. Steber, et al. "Roadmap on dynamics of molecules and clusters in the gas phase". In: *The European Physical Journal D* 75.5 (2021), pp. 1–53.

[6] B. Kafle, O. Aviv, V. Chandrasekaran, O. Heber, M. Rappaport, H. Rubinstein, D. Schwalm, D. Strasser, and D. Zajfman. "Electron detachment and fragmentation of laser-excited rotationally hot Al 4-". In: *Physical Review A* 92.5 (2015), p. 052503.

[7] T. Sommerfeld. "Al 4- cluster anion: Electronic structure, excited states, and electron detachment". In: *The Journal of chemical physics* 132.12 (2010), p. 124305.

[8] A. Schönhals. "Fast decay of highly excited SF6-cluster anions with the CTF". PhD thesis. Ruprecht-Karls-Universität Heidelberg, 2010.

[9] C. Breitenfeldt, K. Blaum, S. George, J. Göck, G. Guzmán-Ramírez, J. Karthein, T. Kolling, M. Lange, S. Menk, C. Meyer, et al. "Long-term monitoring of the internal energy distribution of isolated cluster systems". In: *Physical Review Letters* 120.25 (2018), p. 253001.

[10] R. von Hahn, A. Becker, F. Berg, K. Blaum, C. Breitenfeldt, H. Fadil, F. Fellenberger, M. Froese, S. George, J. Göck, et al. "The cryogenic storage ring CSR". In: *Review of Scientific Instruments* 87.6 (2016), p. 063115.

[11] F. Nüsslein. "An experimental setup for testing ion beam sources for the CSR facility". MA thesis. Ruprecht-Karls-Universität Heidelberg, 2018.

[12] V. C. Schmidt. "Design of an ion beam extraction optics and analysis of the molecular composition of an ion beam in an electrostatic storage ring". BA Thesis. Ruprecht-Karls-Universität Heidelberg, 2018.

[13] E. Heinicke and H. Baumann. "Penning ion source for MP accelerator". In: *Nuclear Instruments and Methods* 74.2 (1969), pp. 229–232.

[14] R. Middleton. "A versatile high intensity negative ion source". In: *Nuclear Instruments and Methods in Physics Research* 214.2-3 (1983), pp. 139–150.

[15] T. G. Dietz, M. A. Duncan, D. E. Powers, and R. E. Smalley. "Laser production of supersonic metal cluster beams". In: *The Journal of Chemical Physics* 74.11 (1981), pp. 6511–6512.

[16] V. Bondybey and J. English. "Laser induced fluorescence of metal clusters produced by laser vaporization: Gas phase spectrum of Pb2". In: *The Journal of Chemical Physics* 74.12 (1981), pp. 6978–6979.

[17] M. A. Duncan. "Invited review article: laser vaporization cluster sources". In: *Review of Scientific Instruments* 83.4 (2012), p. 041101.

[18] A. H. Lutey. "An improved model for nanosecond pulsed laser ablation of metals". In: *Journal of Applied Physics* 114.8 (2013), p. 083108.

[19] J. Karthein. "Preparatory studies for laser experiments on cold metal clusters at the CSR". BA Thesis. Ruprecht-Karls-Universität Heidelberg, 2015.

[20] S. Maruyama, L. R. Anderson, and R. E. Smalley. "Direct injection supersonic cluster beam source for FT-ICR studies of clusters". In: *Review of scientific instruments* 61.12 (1990), pp. 3686–3693.

[21] H. J. Eichler and J. Eichler. *Laser: Bauformen, Strahlführung, Anwendungen*. Springer-Verlag, 2015.

[22] J. Karthein and C. Breitenfeldt. *LVAP-Zusammenfassung*. Internal documentation. 2015.

[23] EKSPLA. *Tunable Nd:YAG-Laser System NT342B-SH-SFG*. 2012.

[24] D. Margarone, L. Torrisi, A. Picciotto, F. Caridi, and S. Gammino. "Production of ion and electron streams by pulsed-laser ablation of Ta and Cu". In: *Radiation Effects & Defects in Solids* 160.10-12 (2005), pp. 515–524.

[25] C. Walker, M. El-Gomati, A. Assa'd, and M. Zadražil. "The secondary electron emission yield for 24 solid elements excited by primary electrons in the range 250–5000 eV: a theory/experiment comparison". In: *Scanning* 30.5 (2008), pp. 365–380.

Erklärung

Ich versichere, dass ich diese Arbeit selbstständig verfasst und keine anderen als die angegebenen Quellen und Hilfsmittel benutzt habe.

Heidelberg, den 11.04.2022,

Danksagung

Diese Arbeit wäre ohne die Unterstützung einer Reihe von Personen nicht möglich gewesen. Euch möchte ich an dieser Stelle nochmal danken.

Danke Felix Nüsslein, für deine großartige und enge Betreuung in den letzten 2 Jahren und insbesondere während dieser Arbeit! Danke, für die unzähligen interessanten Gespräche, für deine Geduld und für dein Vertrauen.

Danke Prof. Dr. Andreas Wolf, dass Du mich damals in die Gruppe geholt hast und für die Zeit die Du Dir während diesem Projekt für mich genommen hast.

Danke Prof. Dr. Robert Moshammer, dass Du dich sofort bereit erklärt hast diese Arbeit zu begutachten.

Danke an euch alle aus der CSR-Gruppe, für die vielen interessanten Gespräche, die schöne Zeit hier und dass ihr immer ein offenes Ohr für Fragen habt.

Danke Manfred König und Maximilan Trebis, dass ihr euch nicht nur schnell und zuverlässig um jedes meiner Anliegen gekümmert habt, sondern das Experiment mit vielen Ideen auch selber mitgestaltet habt.

Danke an euch alle aus der Werkstatt, für das schnelle und sorgfältige Bearbeiten der Aufträge, ganz egal wann und wie oft ich etwas von euch brauchte.

Danke Annika Stark, für das Erstellen der CAD-Modelle.

Danke an meine Freunde, dass ihr immer da seid.

Danke Olga, für die schöne Zeit die tolle Unterstützung und, das, Korrekturlesen.

Danke an meine Familie. Für alles.